Coordination compounds built up from $M^{II}Cl_2$ and 3-cyanopyridine: double chains, single chains and isolated complexes.

Miriam Heine, Lothar Fink, Martin U. Schmidt*

Institute of Inorganic and Analytical Chemistry, Goethe University, Max-von-Laue-Str. 7, 60438 Frankfurt am Main, Germany. E-Mail: m.schmidt@chemie.uni-frankfurt.de; Fax: +49 69798 29235; Tel: +49 69798 29123

Figures

Tables

Experimental details

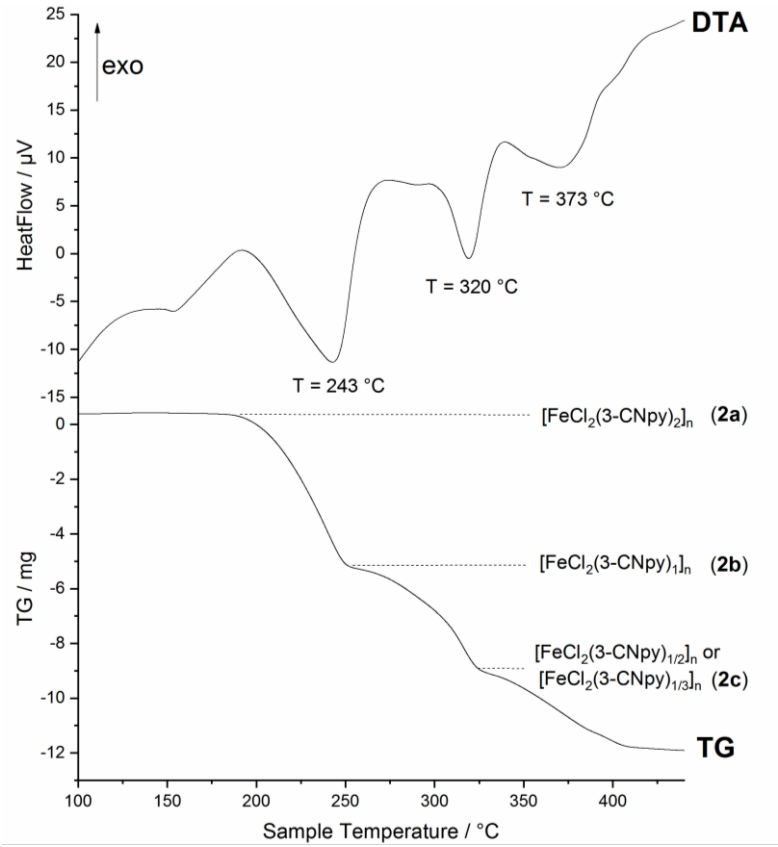

Figure S1. DTA/TG curves of $[FeCl_2(3\text{-}CNpy)_2]_n$ (**2a**). Heating rate: 5 K/min, Ar atmosphere, Al_2O_3 crucible. * DTA-TG results point to the formation of $[FeCl_2(3\text{-}CNpy)_{1/2}]_n$ or $[FeCl_2(3\text{-}CNpy)_{1/3}]_n$, see Tab. S1 in this document.

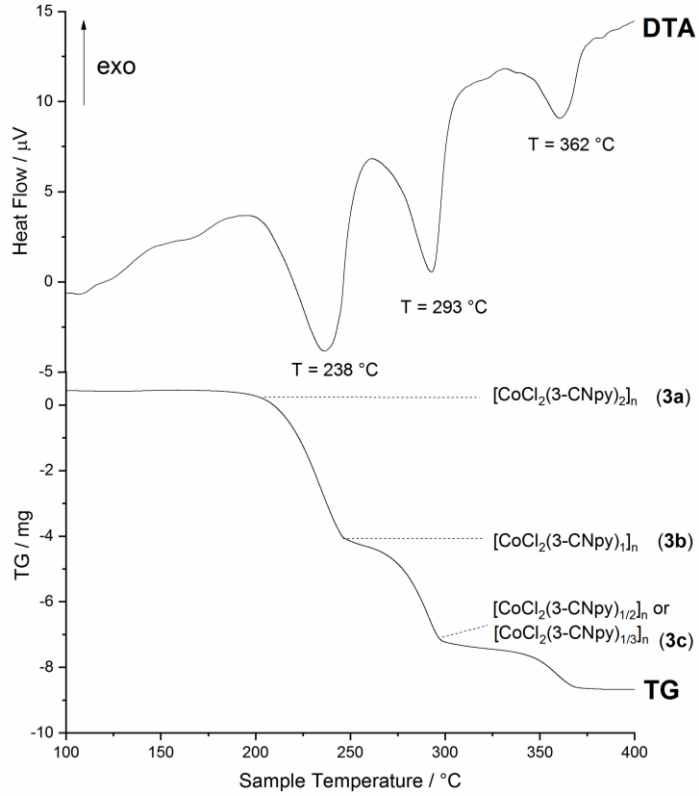

Figure S2. DTA/TG curves of $[CoCl_2(3\text{-}CNpy)_2]_n$ (**3a**). Heating rate: 5 K/min, Ar atmosphere, Al_2O_3 crucible. * DTA-TG results point to the formation of $[CoCl_2(3\text{-}CNpy)_{1/2}]_n$ or $[CoCl_2(3\text{-}CNpy)_{1/3}]_n$, see Tab. S1 in this document.

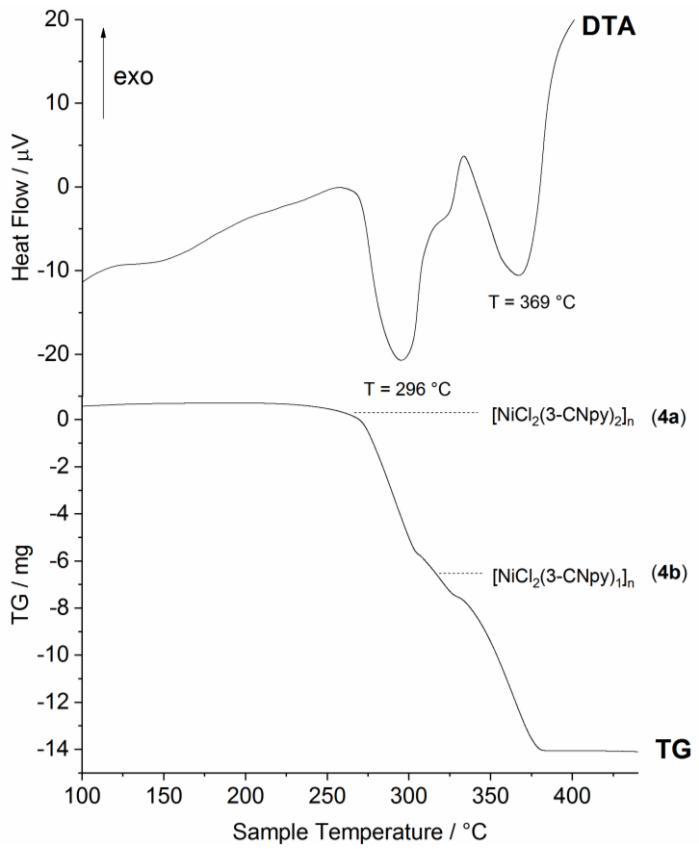

Figure S3. DTA/TG curves of $[NiCl_2(3\text{-}CNpy)_2]_n$ (**4a**). Heating rate: 5 K/min, Ar atmosphere, Al_2O_3 crucible.

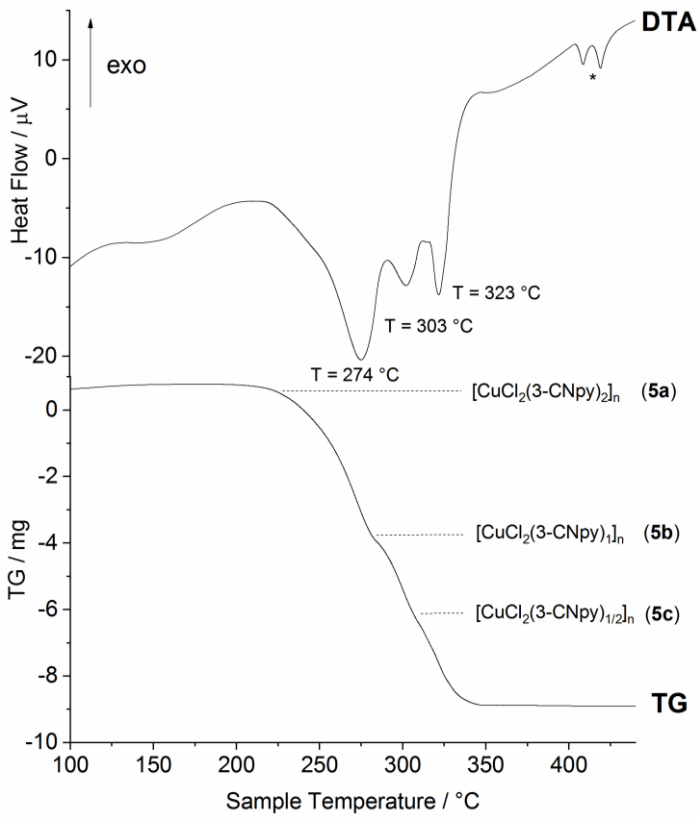

Figure S4. DTA/TG curves of $[CuCl_2(3\text{-}CNpy)_2]_n$ (**5a**). Heating rate: 5 K/min, Ar atmosphere, Al_2O_3 crucible. The endothermic signals marked by the may be attributed to the partial formation of anhydrous CuCl, see Fig. S28 in this document.

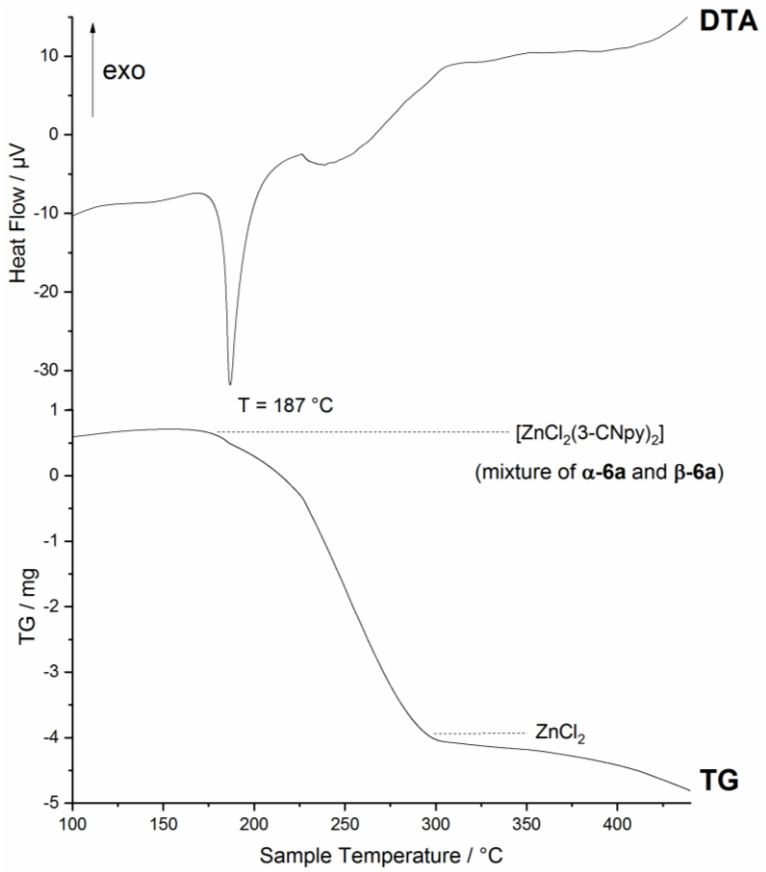

Figure S5. DTA/TG curves of $[ZnCl_2(3\text{-}CNpy)_2]$ (mixture of **α-6a** and **β-6a**). Heating rate: 5 K/min, Ar atmosphere, Al_2O_3 crucible.

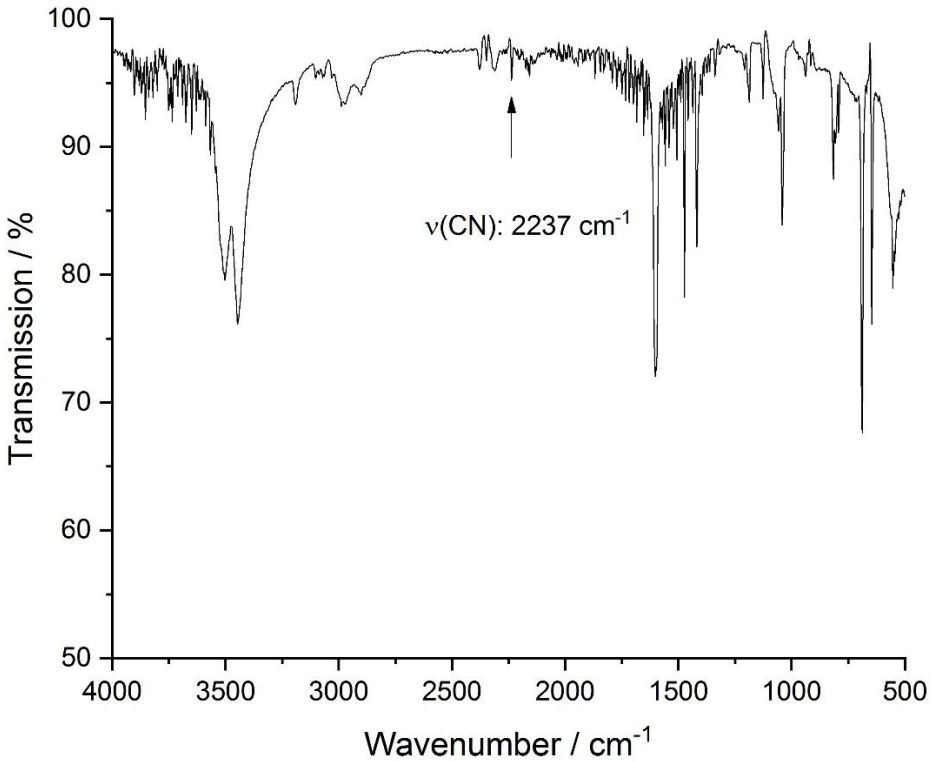

Figure S6. IR spectrum of $[MnCl_2(3\text{-}CNpy)_2]_n$ (**1a**).

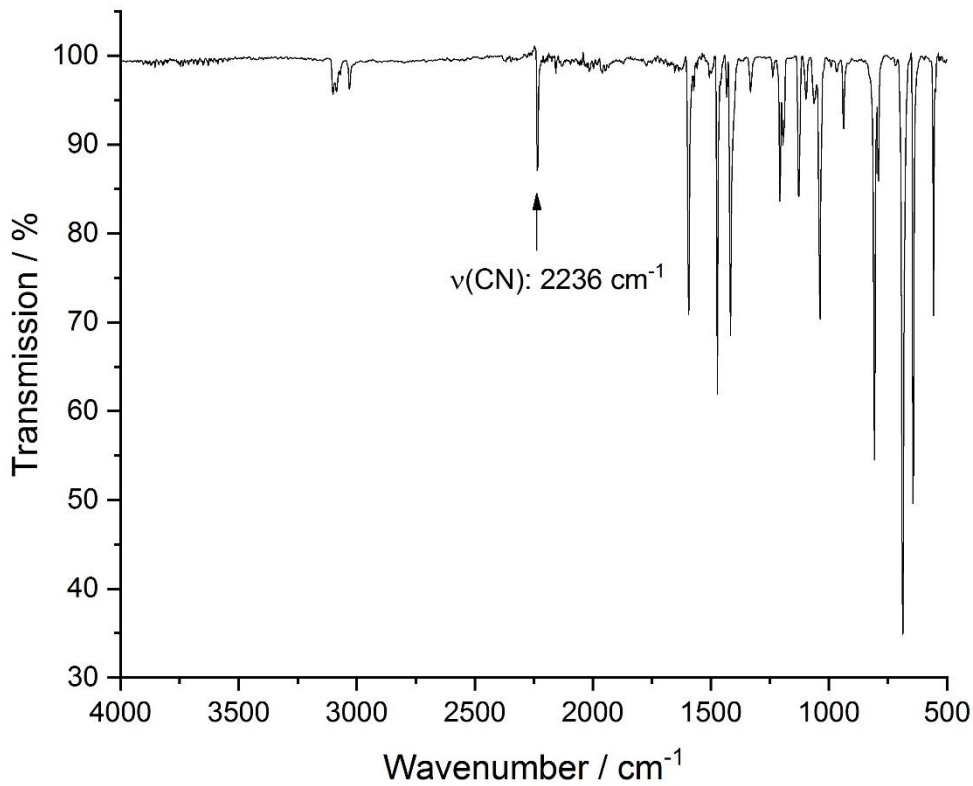

Figure S7. IR spectrum of $[MnCl_2(3\text{-}CNpy)_1]_n$ (**1b**).

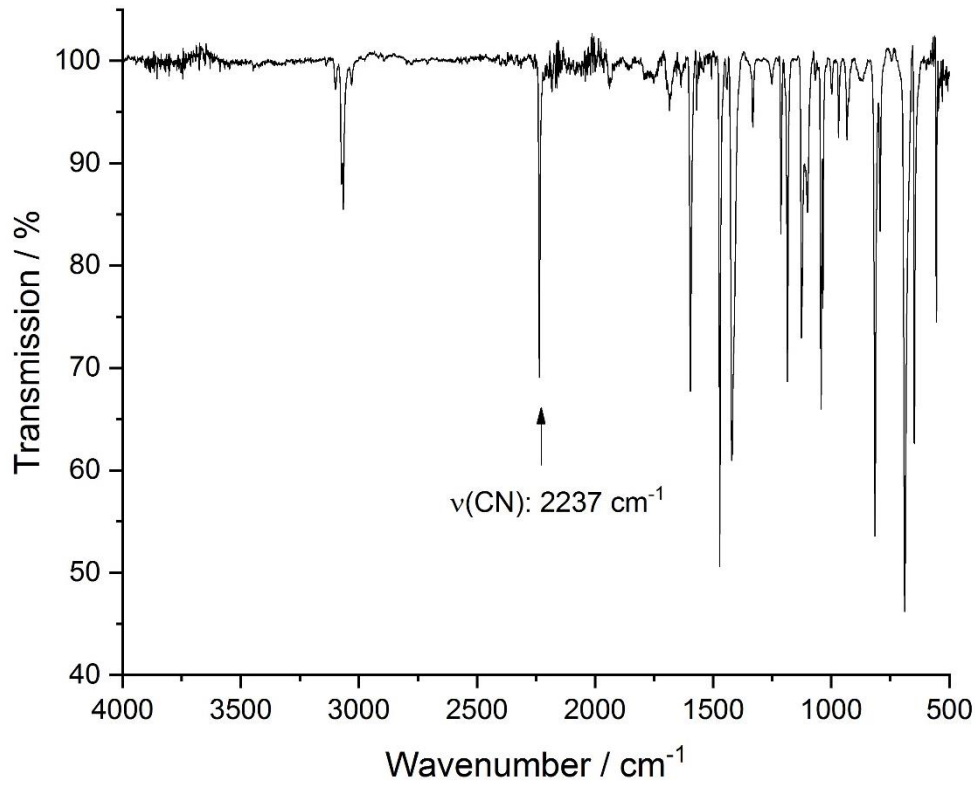

Figure S8. IR spectrum of $[FeCl_2(3\text{-}CNpy)_2]_n$ (**2a**).

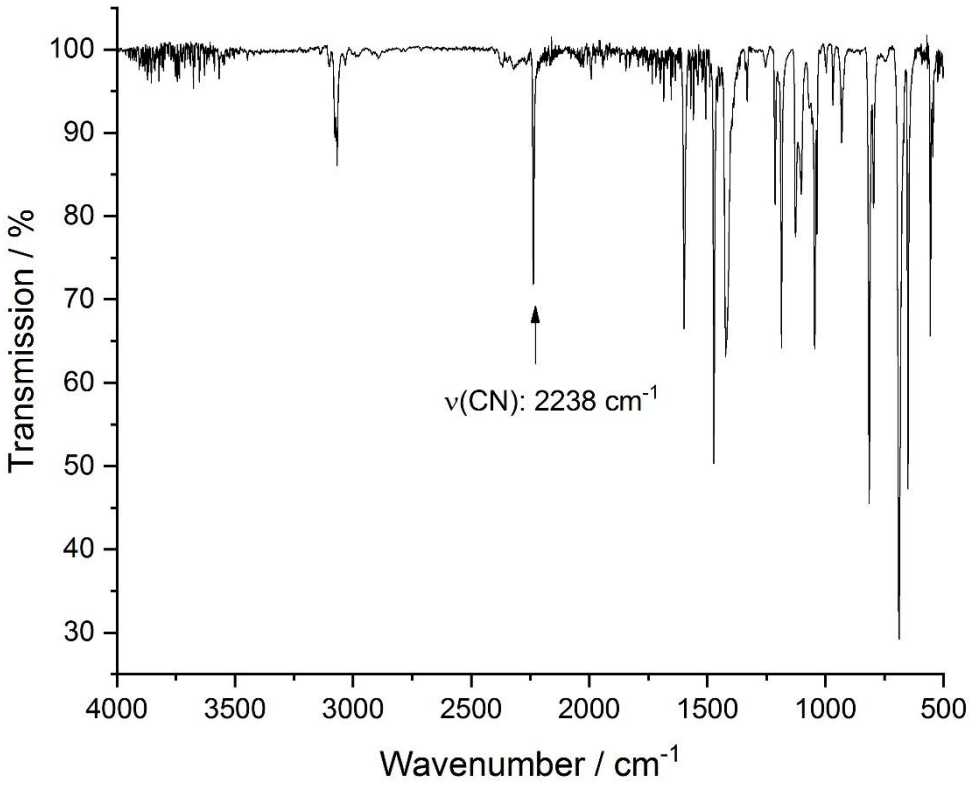

Figure S9. IR spectrum of $[CoCl_2(3\text{-}CNpy)_2]_n$ (**3a**).

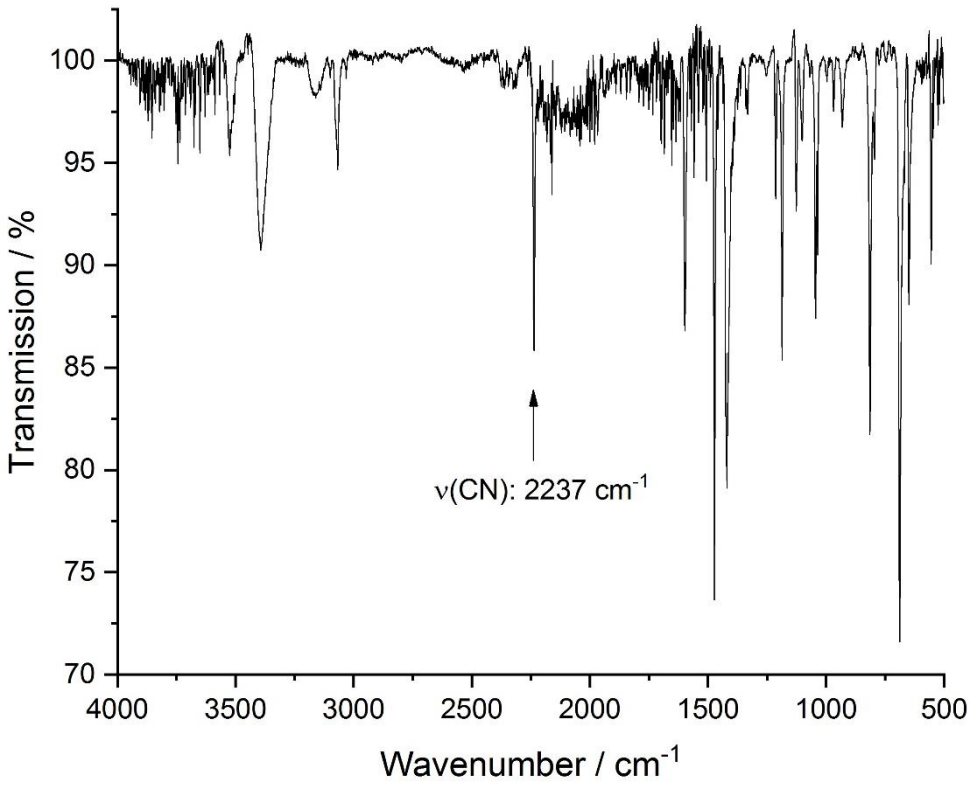

Figure S10. IR spectrum of $[CoCl_2(3\text{-}CNpy)_1]_n$ (**3b**).

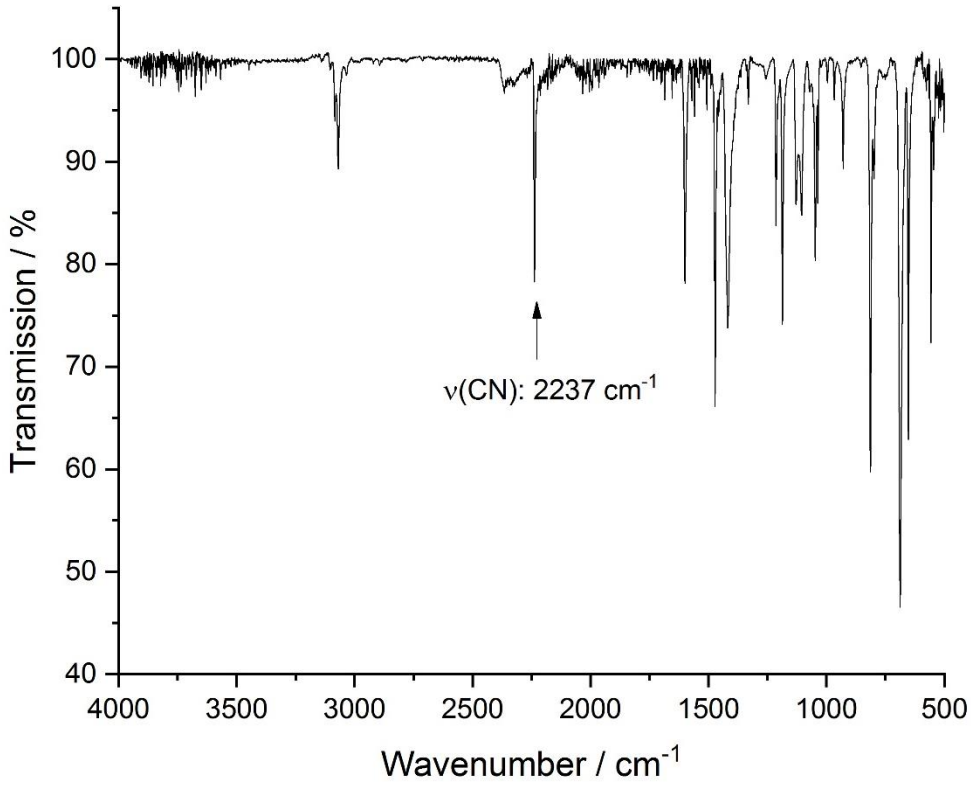

Figure S11. IR spectrum of $[NiCl_2(3\text{-}CNpy)_2]_n$ (**4a**).

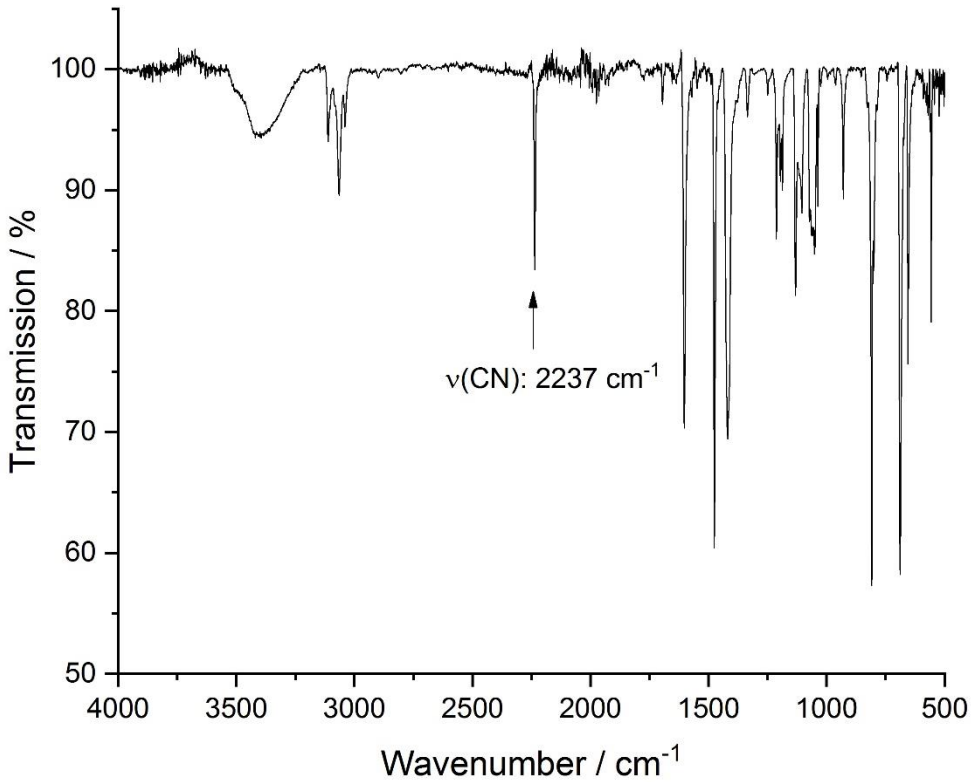

Figure S12. IR spectrum of $[NiCl_2(3\text{-}CNpy)_1]_n$ (**4b**).

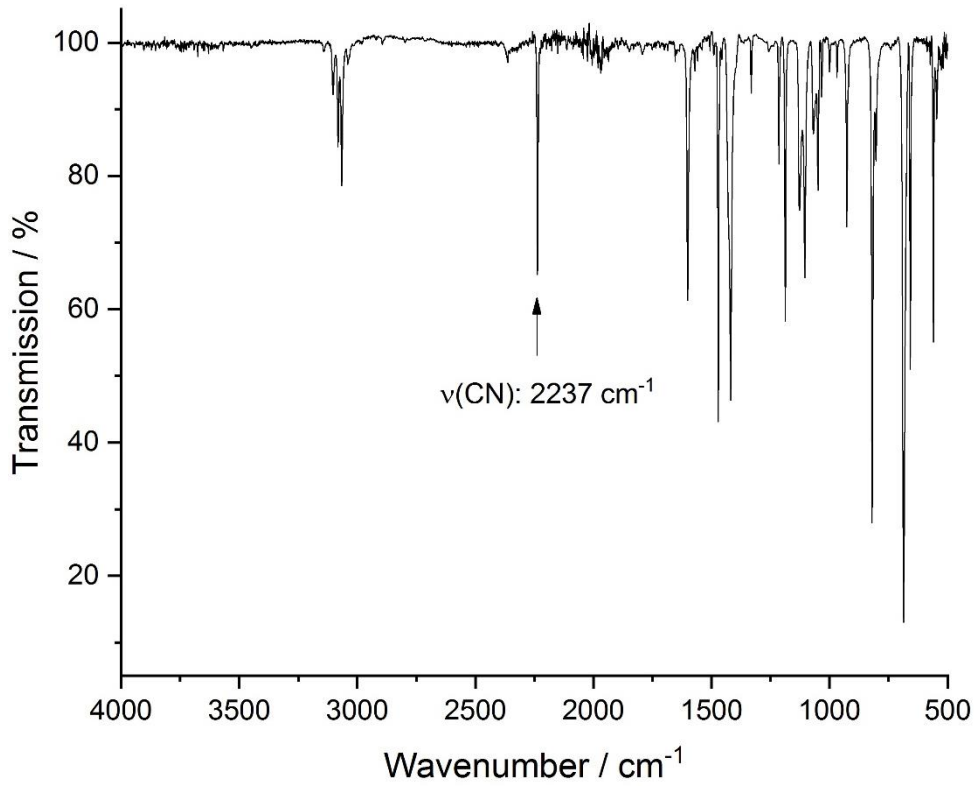

Figure S13. IR spectrum of $[CuCl_2(3\text{-}CNpy)_2]_n$ (**5a**).

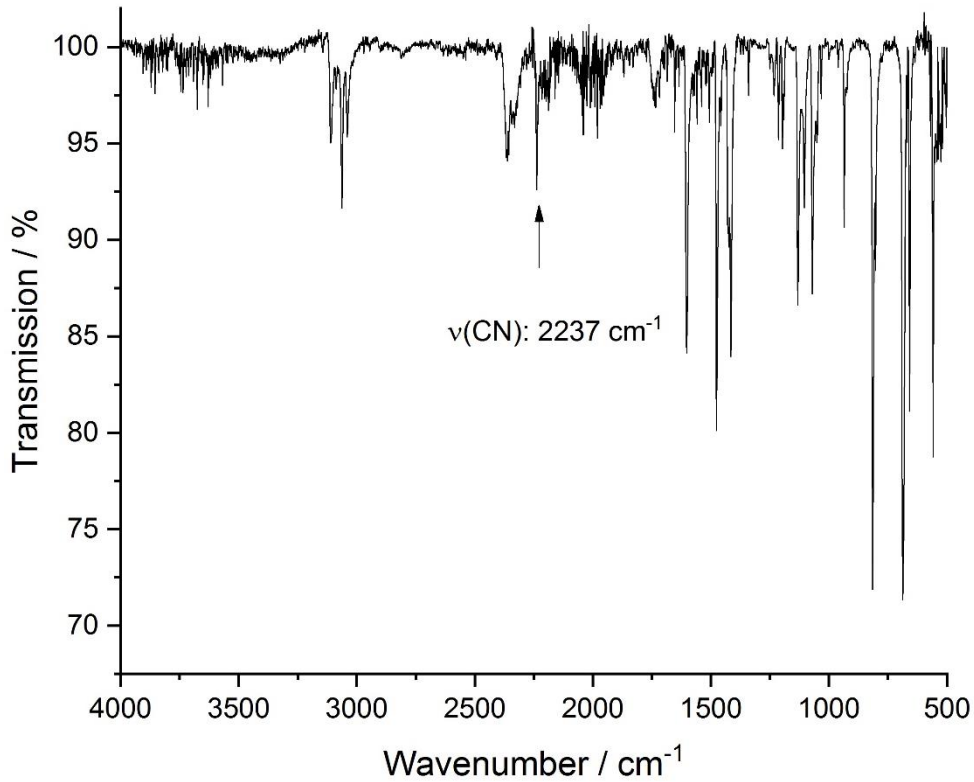

Figure S14. IR spectrum of $[CuCl_2(3\text{-}CNpy)_1]_n$ (**5b**).

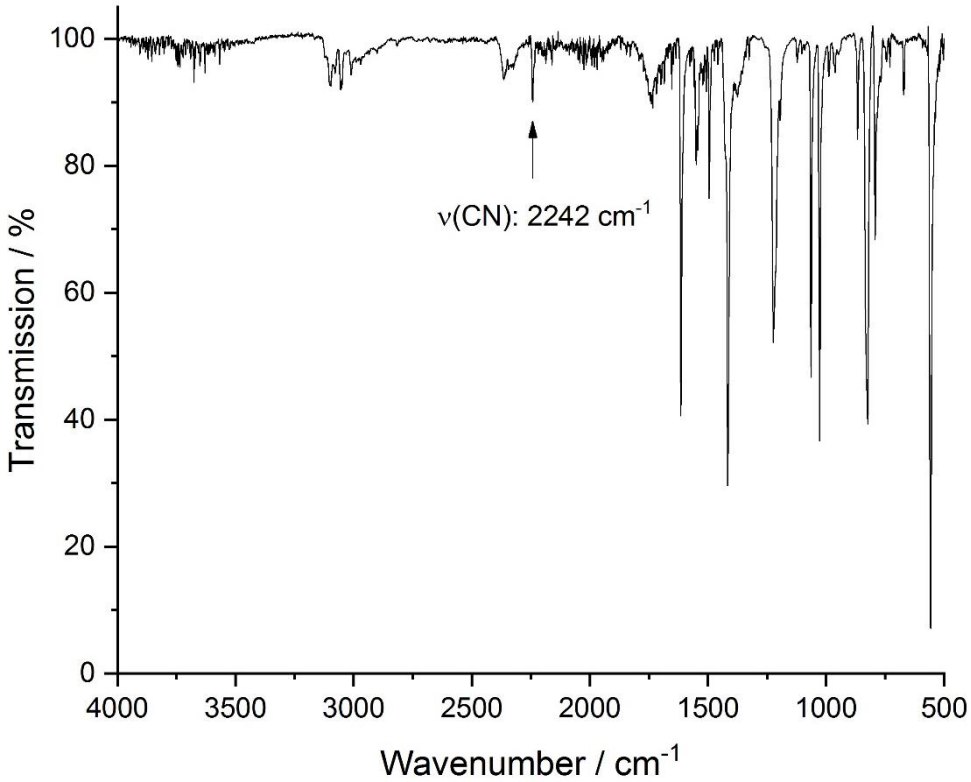

Figure S15. IR spectrum of $[ZnCl_2(3\text{-}CNpy)_2]$: mixture of **α-6** and **β-6**.

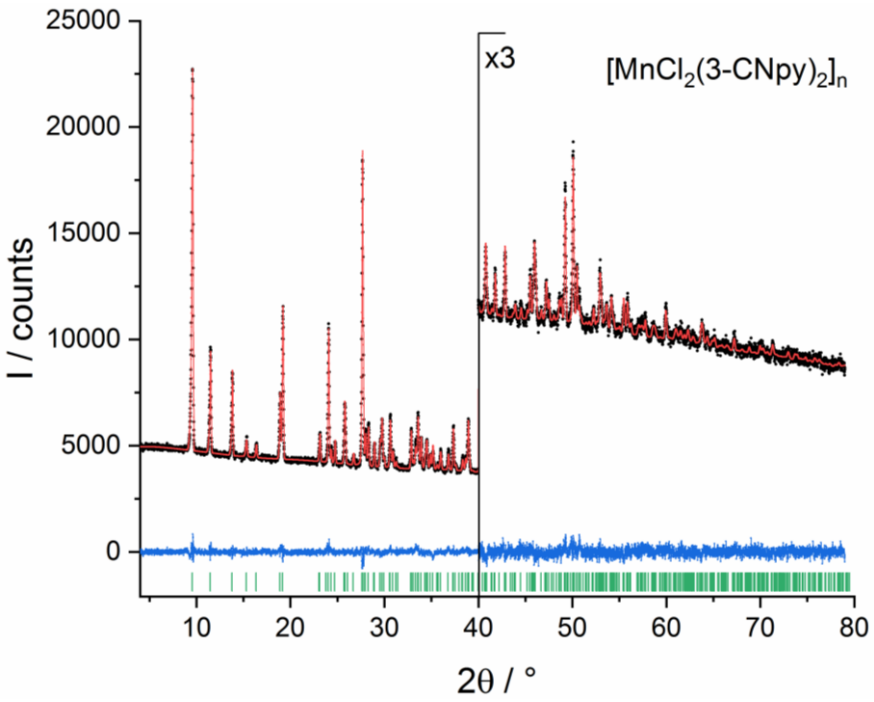

Figure S16. Rietveld plot of $[MnCl_2(3\text{-}CNpy)_2]_n$ (**1a**). Observed powder diagram (black points), simulated powder diagram (red solid line), difference profile (blue solid line) and reflection positions (green tick marks). Change of the scales with corresponding factors is indicated in the diagrams.

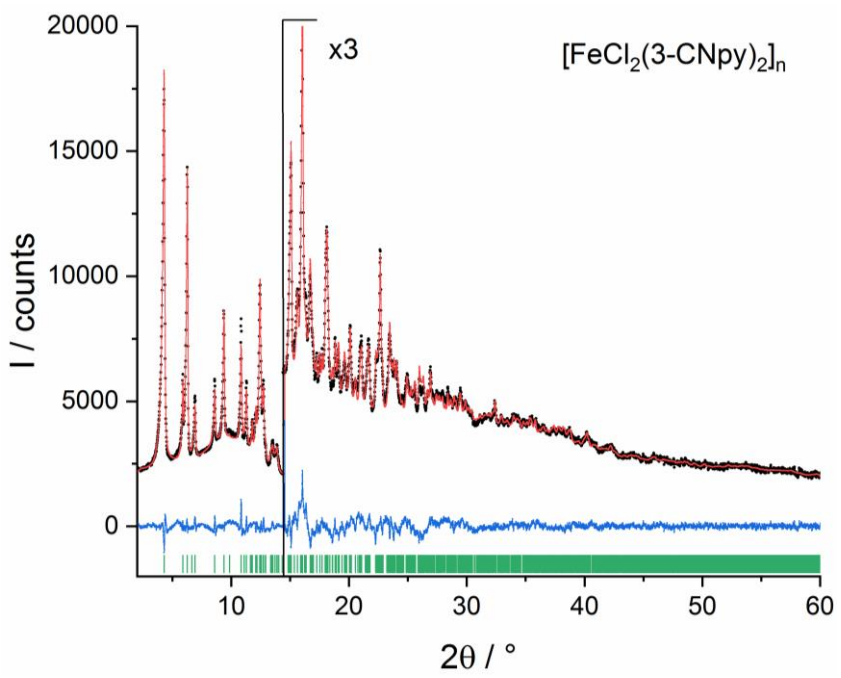

Figure S17. Rietveld plot of $[FeCl_2(3\text{-}CNpy)_2]_n$ (**2a**). Observed powder diagram (black points), simulated powder diagram (red solid line), difference profile (blue solid line) and reflection positions (green tick marks). Change of the scales with corresponding factors is indicated in the diagrams. XRPD data were collected with Mo $K\alpha_1$ radiation.

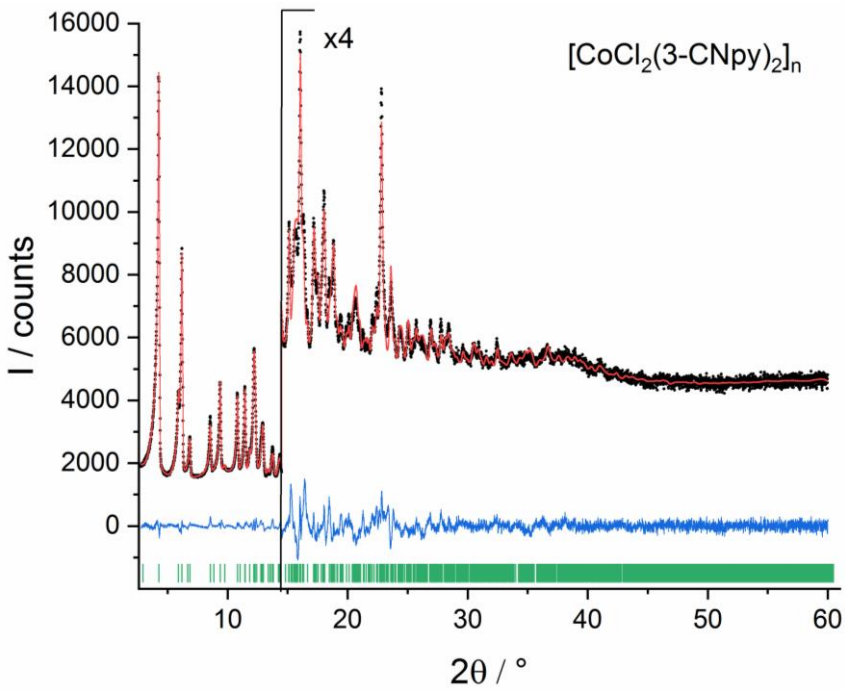

Figure S18. Rietveld plot of $[CoCl_2(3\text{-}CNpy)_2]_n$ (**3a**). Observed powder diagram (black points), simulated powder diagram (red solid line), difference profile (blue solid line) and reflection positions (green tick marks). Change of the scales with corresponding factors is indicated in the diagrams. XRPD data were collected with Mo $K\alpha_1$ radiation.

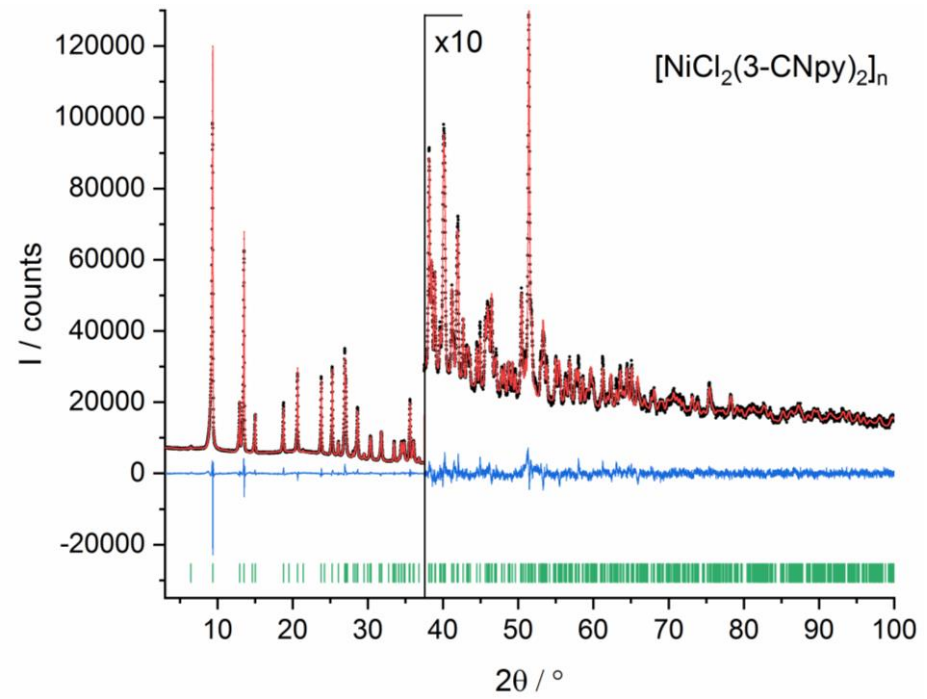

Figure S19. Rietveld plot of $[NiCl_2(3\text{-}CNpy)_2]_n$ (**4a**). Observed powder diagram (black points), simulated powder diagram (red solid line), difference profile (blue solid line) and reflection positions (green tick marks). Change of the scales with corresponding factors is indicated in the diagrams.

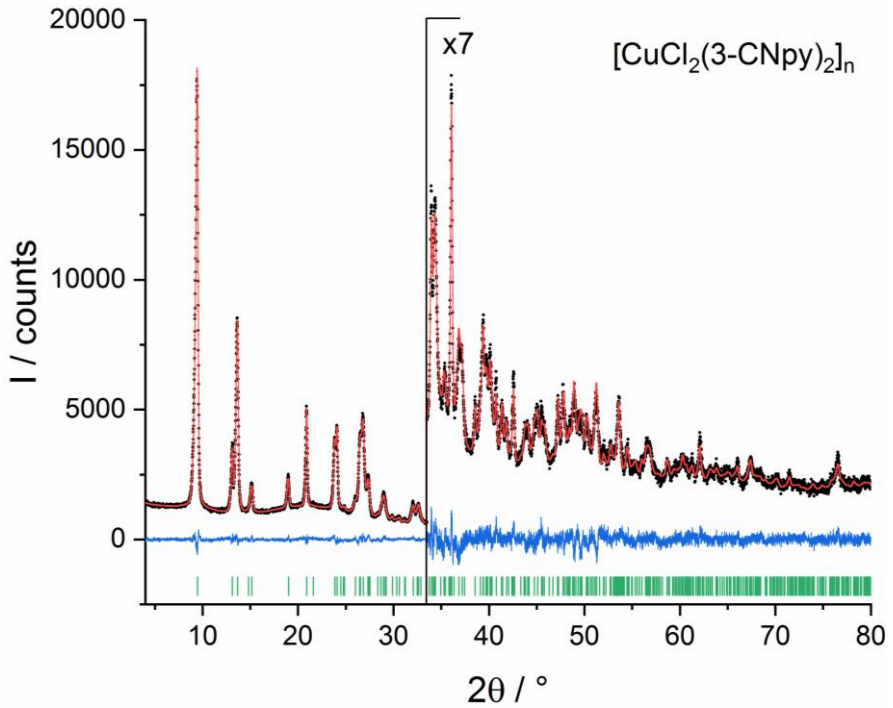

Figure S20. Rietveld plot of $[CuCl_2(3\text{-}CNpy)_2]_n$ (**5a**). Observed powder diagram (black points), simulated powder diagram (red solid line), difference profile (blue solid line) and reflection positions (green tick marks). Change of the scales with corresponding factors is indicated in the diagrams.

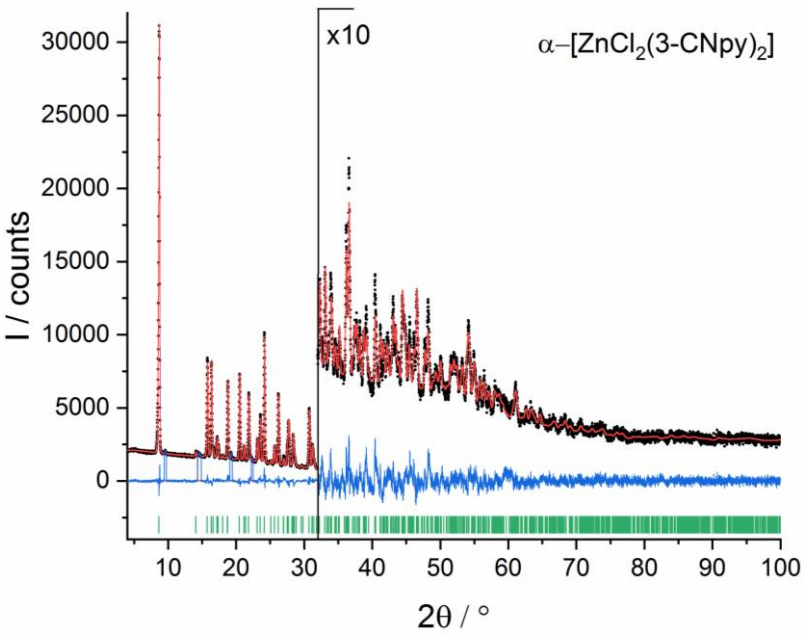

Figure S21. Rietveld plot of α-[$ZnCl_2$(3-CNpy)$_2$] (**α-6a**). Observed powder diagram (black points), simulated powder diagram (red solid line), difference profile (blue solid line) and reflection positions (green tick marks). Reflections of **β-6a** are excluded. Change of the scales with corresponding factors is indicated in the diagrams.

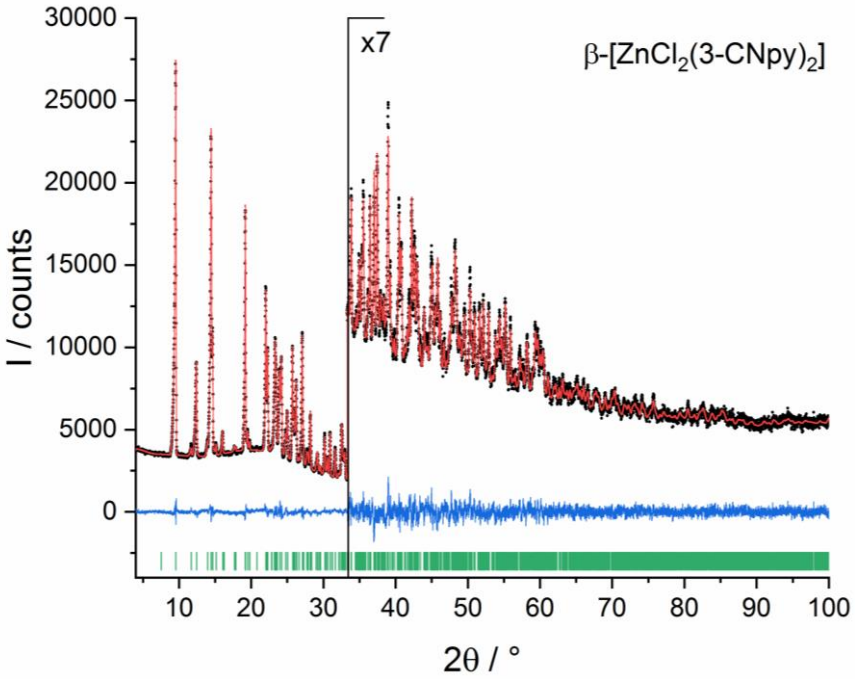

Figure S22. Rietveld plot of β-[$ZnCl_2$(3-CNpy)$_2$] (**β-6a**). Observed powder diagram (black points), simulated powder diagram (red solid line), difference profile (blue solid line) and reflection positions (green tick marks). Change of the scales with corresponding factors is indicated in the diagrams.

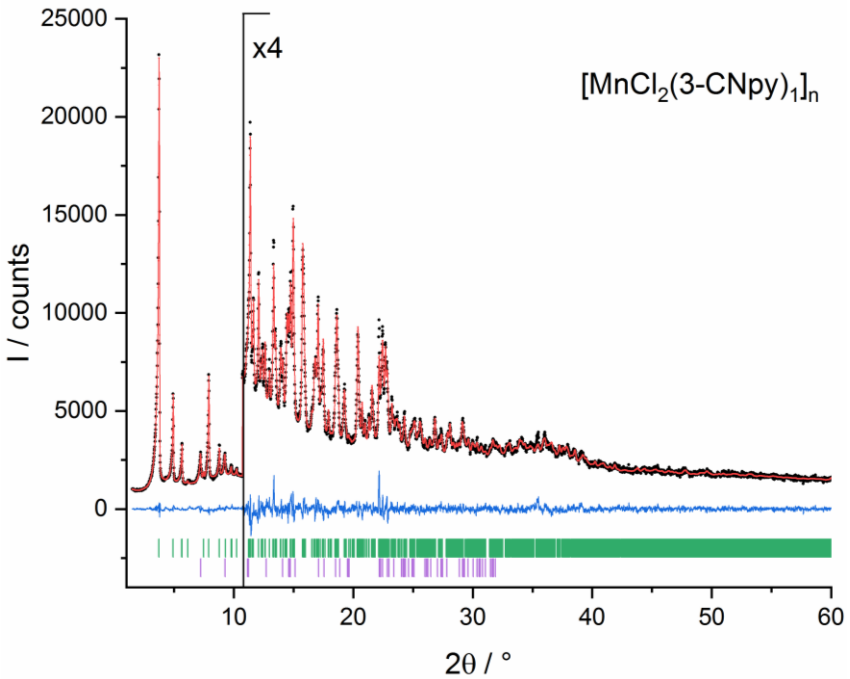

Figure S23. Rietveld plot of $[MnCl_2(3\text{-}CNpy)_1]_n$ (**1b**). Observed powder diagram (black points), simulated powder diagram (red solid line), difference profile (blue solid line) and reflection positions (green tick marks). Change of the scales with corresponding factors is indicated in the diagrams. Reflection positions of $[MnCl_2(3\text{-}CNpy)_{1/3}]_n$ (**1c**) are shown in violet.

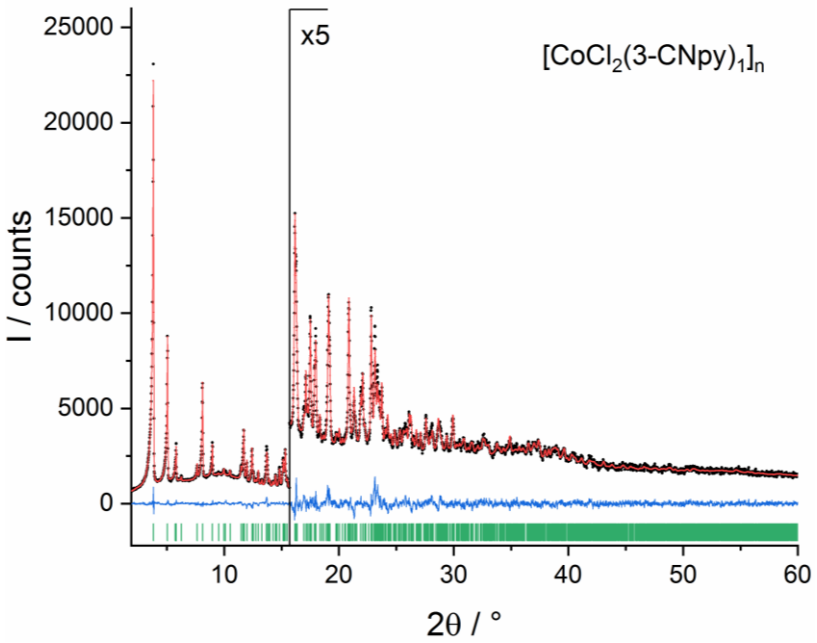

Figure S24. Rietveld plot of $[CoCl_2(3\text{-}CNpy)_1]_n$ (**3b**). Observed powder diagram (black points), simulated powder diagram (red solid line), difference profile (blue solid line) and reflection positions (green tick marks). Change of the scales with corresponding factors is indicated in the diagrams. XRPD data were collected with Mo $K\alpha_1$ radiation.

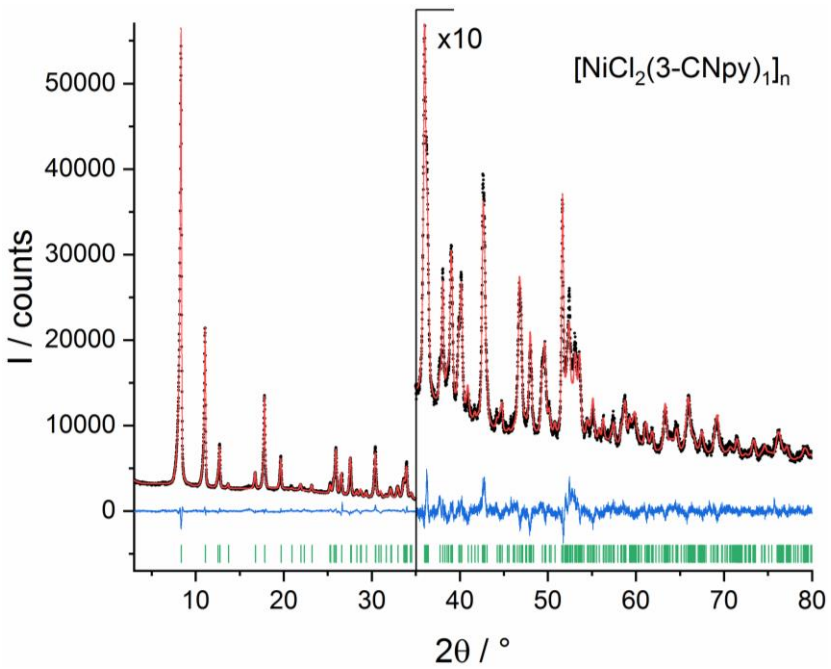

Figure S25. Rietveld plot of $[NiCl_2(3\text{-}CNpy)_1]_n$ (**4b**). Observed powder diagram (black points), simulated powder diagram (red solid line), difference profile (blue solid line) and reflection positions (green tick marks). Change of the scales with corresponding factors is indicated in the diagrams.

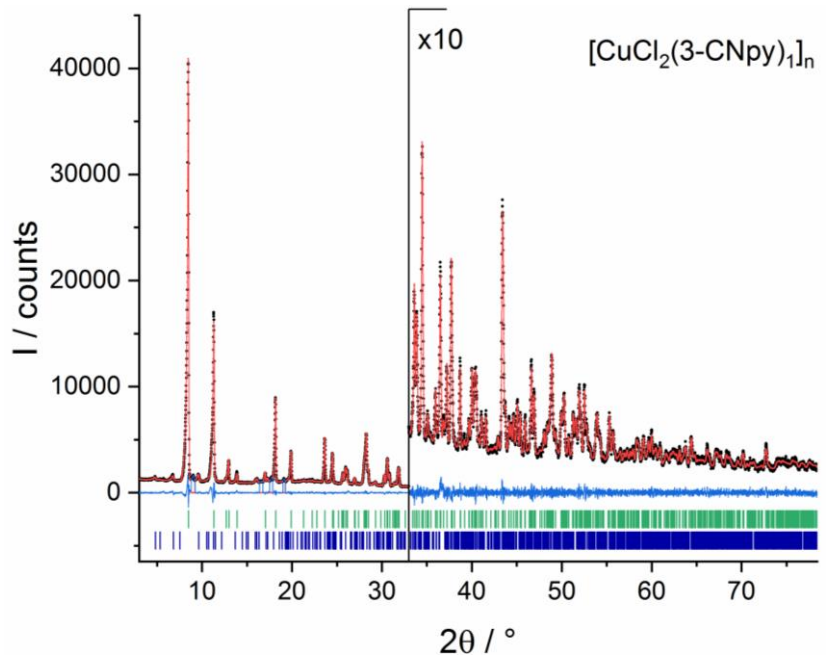

Figure S26. Rietveld plot of $[CuCl_2(3\text{-}CNpy)_1]_n$ (**5b**). Observed powder diagram (black points), simulated powder diagram (red solid line), difference profile (blue solid line) and reflection positions (green tick marks). Reflection positions of $[CuCl_2(3\text{-}CNpy)_{1/2}]_n$ (**5c**) are shown in dark blue. Reflections of a further foreign phase are excluded. Change of the scales with corresponding factors is indicated in the diagram.

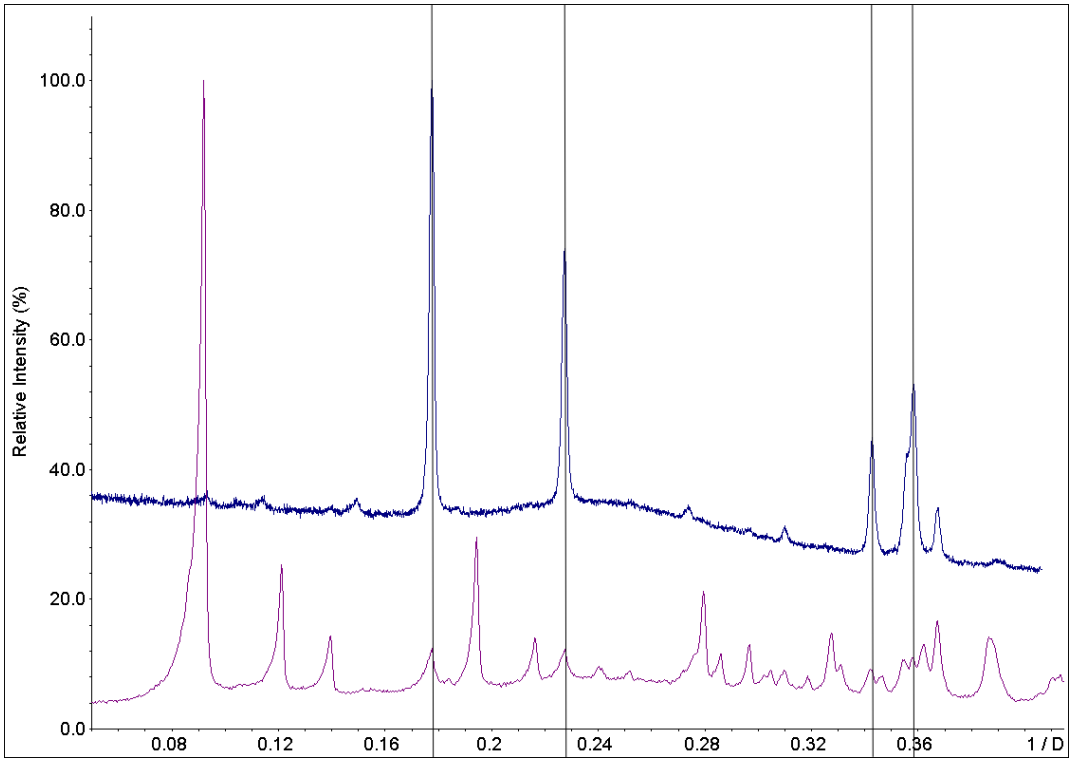

Figure S27. XRPD of $[MnCl_2(3\text{-}CNpy)_1]_n$ (**1b**) (violet pattern) containing foreign reflections (grey lines) of $[MnCl_2(3\text{-}CNpy)_{1/3}]_n$ (**1c**) (blue pattern); reflections XRPD data of **1b** were collected with Mo $K\alpha_1$ radiation. XRPD data of **1c** were collected with Cu $K\alpha_1$ radiation.

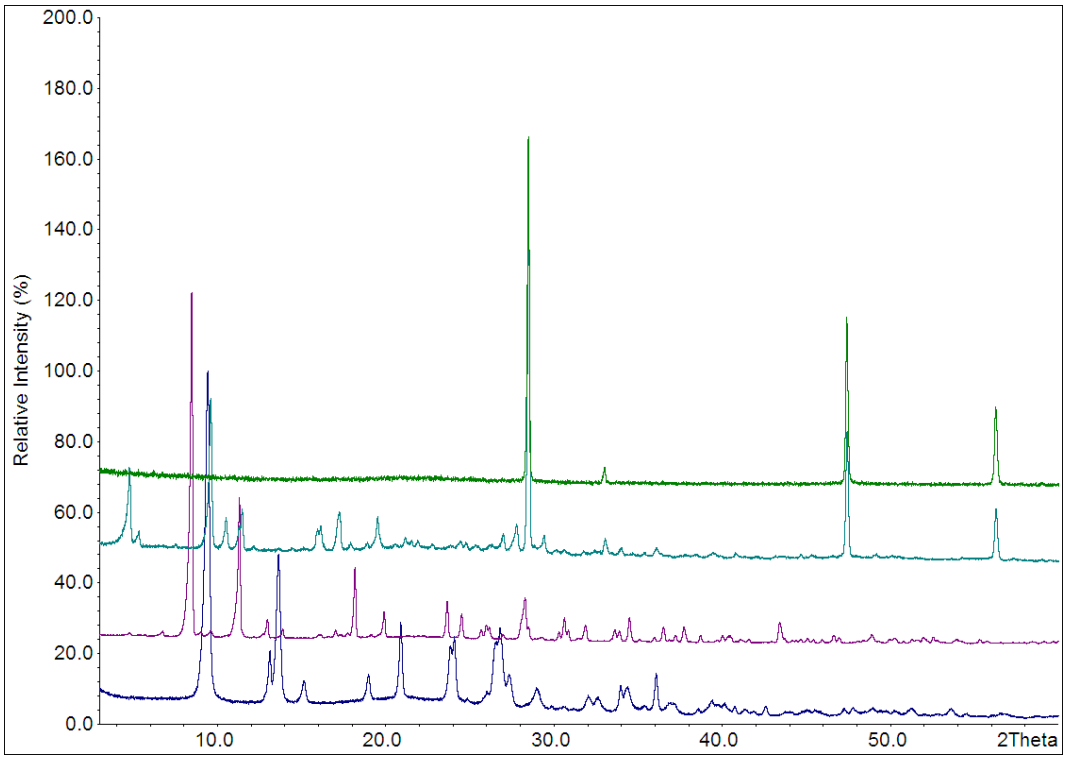

Figure S28. XRPD of the Cu series, showing $[CuCl_2(3\text{-}CNpy)_2]_n$ (**5a**), blue pattern; $[CuCl_2(3\text{-}CNpy)_1]_n$ (**5b**) violet, $[CuCl_2(3\text{-}CNpy)_{1/2}]_n$ (**5c**), light green; and CuCl, dark green (top). XRPD of **5b** contains foreign reflections of **5c**. Further thermal decomposition is accompanied by the formation of CuCl.

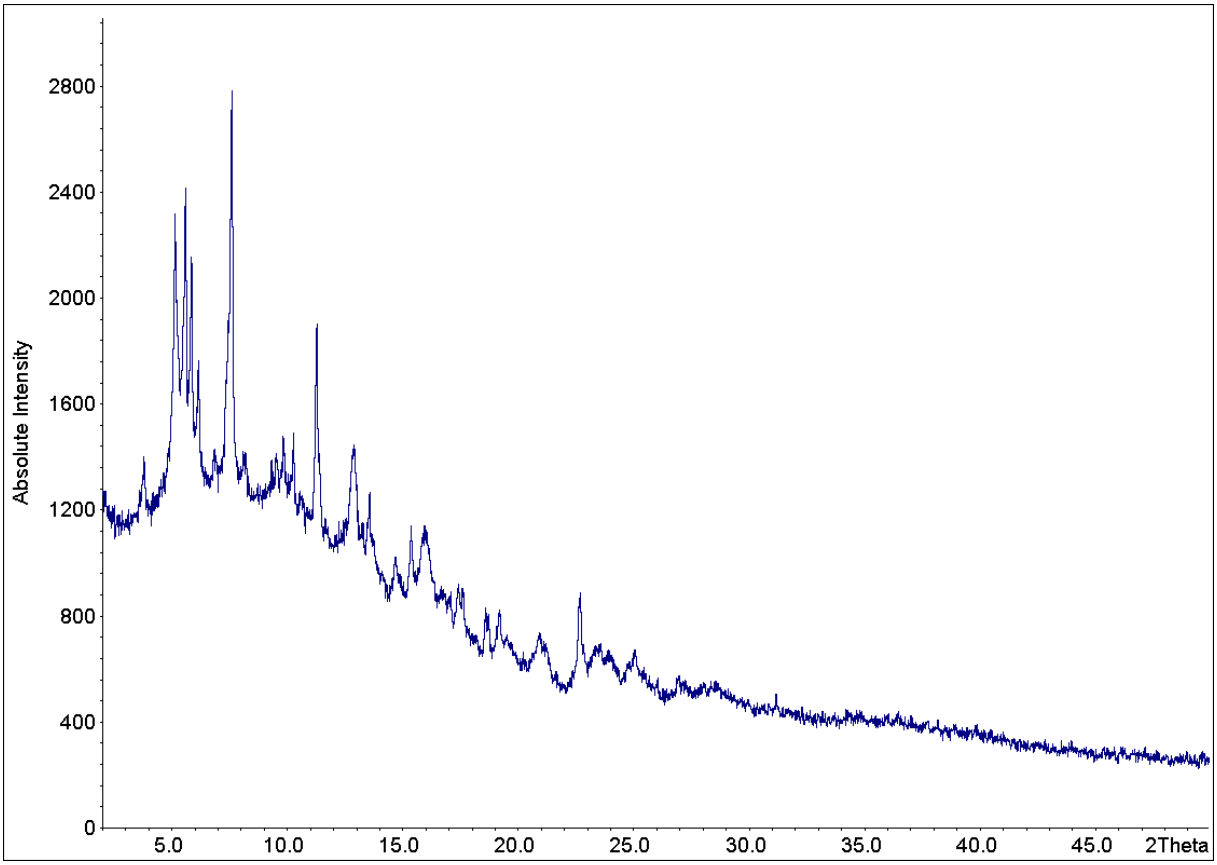

Figure S29. XRPD of $[FeCl_2(3\text{-}CNpy)_1]_n$ (**2b**). The data were collected with Mo $K\alpha_1$ radiation. The structure solution has not been successful.

Table S1. Results of DTA/TG measurements of $[M^{II}Cl_2(3\text{-CNpy})_2]$ (M^{II} = Mn, Fe, Co, Ni, Cu, Zn). T: DTA peak temperatures, m_0: weight of starting compound, Δm_{exp}: relative experimental weight loss, experimental $\Delta m_{exp}/m_0$, calculated $\Delta m_{cal}/m_0$.

Compound	T / °C	m_0 / mg	Δm_{exp} / mg	$\Delta m_{exp}/m_0$ / %	$\Delta m_{cal}/m_0$ / %
(**1**)					
$[MnCl_2(3\text{-CNpy})_2]_n$		34.44	0	0	0
$[MnCl_2(3\text{-CNpy})_1]_n$	246.9		10.49	30.47	31.16
$[MnCl_2(3\text{-CNpy})_{1/3}]_n$	302.4		7.27	30.34	30.18
$MnCl_2$	370.9		2.94	17.59	21.61
(**2**)					
$[FeCl_2(3\text{-CNpy})_2]_n$		23.06	0	0	0
$[FeCl_2(3\text{-CNpy})_1]_n$	243.4		5.62	24.49	31.08
$[FeCl_2(3\text{-CNpy})_{1/2}]_n$	319.6		3.78	21.66	22.52
$FeCl_2$	373.4		2.76	19.72	29.11
$[FeCl_2(3\text{-CNpy})_1]_n$	243.4		5.62	24.49	31.08
$[FeCl_2(3\text{-CNpy})_{1/3}]_n$	319.6		3.78	21.66	30.07
$FeCl_2$	373.4		2.76	19.72	21.49
(**3**)					
$[CoCl_2(3\text{-CNpy})_2]_n$		16.03	0	0	0
$[CoCl_2(3\text{-CNpy})_1]_n$	237.6		4.51	28.13	30.79
$[CoCl_2(3\text{-CNpy})_{1/3}]_n$	293.4		2.99	25.92	29.67
$CoCl_2$	361.8		1.11	12.98	21.09
$[CoCl_2(3\text{-CNpy})_1]_n$	237.6		4.51	28.13	30.79
$[CoCl_2(3\text{-CNpy})_{1/2}]_n$	293.4		2.99	25.92	22.25
$CoCl_2$	361.8		1.11	12.98	28.62
(**4**)					
$[NiCl_2(3\text{-CNpy})_2]_n$		24.64	0	0	0
$[NiCl_2(3\text{-CNpy})_1]_n$	295.7		6.054	24.57	30.82
$NiCl_2$	368.9		6.429	34.58	44.55
(**5**)					
$[CuCl_2(3\text{-CNpy})_2]_n$		14.616			
$[CuCl_2(3\text{-CNpy})_1]_n$	274.7		4.62	31.61	30.38
$[CuCl_2(3\text{-CNpy})_{1/2}]_n$	302.9		2.57	25.71	21.81
$CuCl_2$	323.0		2.39	32.18	27.91
(**6**)					
$[ZnCl_2(3\text{-CNpy})_2]$		13.56	0	0	0
$ZnCl_2$	187.0		4.80	35.44	60.43

Table S2 - Part 1. Crystallographic data of $[M^{II}Cl_2(3\text{-}CNpy)_2]_n$ (**1a**-**4a**).

	1a	**2a**	**3a**	**4a**
Compound	$[MnCl_2(3\text{-}CNpy)_2]_n$	$[FeCl_2(3\text{-}CNpy)_2]_n$	$[CoCl_2(3\text{-}CNpy)_2]_n$	$[NiCl_2(3\text{-}CNpy)_2]_n$
CCDC number/ CSD code	1904113	1904107	1904105	1904110
Structure determined from	Powder	Powder	Powder	Powder
Formula	$C_{12}H_8Cl_2MnN_4$	$C_{12}H_8Cl_2FeN_4$	$C_{12}H_8Cl_2CoN_4$	$C_{12}H_8Cl_2NiN_4$
MW /g·mol^{-1}	334.06	334.96	338.05	337.81
Crystal system	Monoclinic	Monoclinic	Monoclinic	Monoclinic
Space group (No.)	$P\,2_1/c$ (14)	$P\,2_1/c$ (14)	$C\,c$ (9)	$C\,c$ (9)
***a* /Å**	3.7030(4)	3.6440(2)	3.6186(2)	3.5837(3)
***b* /Å**	15.4310(4)	13.8135(8)	27.504(2)	27.2889(3)
***c* /Å**	11.5780(3)	13.1192(11)	13.2081(12)	13.1815(3)
***α* /°**	90	90	90	90
***ß* /°**	91.438(2)	98.532(7)	97.49(2)	97.715(4)
***γ* /°**	90	90	90	90
***V* /Å^3**	661.3(6)	653.0(8)	1302.6(9)	1277.4(2)
Z, Z'	2, ½	2, ½	4, 1	4, 1
Site symmetry of M^{II}	$\bar{1}$	$\bar{1}$	1	1
T /K	298	298	298	298
Radiation type	Cu $K\alpha_1$	Mo $K\alpha_1$	Mo $K\alpha_1$	Cu $K\alpha_1$
Wavelength /Å	1.54056	0.70930	0.70930	1.54056
$2\Theta_{min}$ /°	3	1	1	3
$2\Theta_{max}$ /°	80	60	60	100
psd step in 2Θ /°	0.2	1.1	0.2	0.2
time/step / sec	140	900	150	160
number of scans	1	3	8	1
R_p /%	1.411	2.771	2.348	2.665
R_{wp} /%	1.805	3.448	3.179	3.140
R_{exp} /%	1.562	2.260	2.468	1.617
GOF	1.156	1.525	1.288	1.942
R_p' /% [a]	18.327	11.862	11.525	9.804
R_{wp}' /% [a]	12.477	11.391	10.777	10.094
R_{exp}' /% [a]	10.796	7.467	8.365	5.197
a) R_p', R_{wp}' and R_{exp}' values are background corrected according to the reference [38].				

Table S2 - Part 2. Crystallographic data of $[M^{II}Cl_2(3\text{-}CNpy)_2]_{(n)}$ (**5a, α-6a, β-6a**).

	5a	**5a [20]**	**α-6a**	**β-6a**
Compound	$[CuCl_2(3\text{-}CNpy)_2]_n$	$[CuCl_2(3\text{-}CNpy)_2]_n$	$[ZnCl_2(3\text{-}CNpy)_2]$	$[ZnCl_2(3\text{-}CNpy)_2]$
CCDC number/ CSD code	1904106	UTIHAH	1904111	1904112
Structure determined from	Powder	Single crystal	Powder	Powder
Formula	$C_{12}H_8Cl_2CuN_4$	$C_{12}H_8Cl_2CuN_4$	$C_{12}H_8Cl_2ZnN_4$	$C_{12}H_8Cl_2ZnN_4$
MW /g·mol^{-1}	342.67	342.67	334.53	334.53
Crystal system	Monoclinic	Monoclinic	Orthorhombic	Monoclinic
Space group (No.)	$P\ 2_1/c$ (14)	$P\ 2_1/c$ (14)	$P\ nma$ (62)	$P\ 2_1/c$ (14)
***a* /Å**	3.7560(1)	3.710(2)	10.6653(3)	11.6619(15)
***b* /Å**	13.4653(3)	13.420(4)	20.3998(5)	15.0731(18)
***c* /Å**	13.0443(5)	12.987(2)	6.6114(17)	8.0572(10)
***α* /°**	90	90	90	90
***ß* /°**	97.347(3)	97.48(?)	90.0	91.0112(9)
***γ* /°**	90	90	90	90
***V* /Å^3**	654.3(4)	641.0(9)	1438.4(6)	1416.0(7)
Z, Z'	2, ½	2, ½	4, ½	4, 1
Site symmetry of M^{II}	$\bar{1}$	$\bar{1}$	*.m.*	1
T /K	298	123	298	298
Radiation type	Cu $K\alpha_1$	Mo $K\alpha$	Cu $K\alpha_1$	Cu $K\alpha_1$
Wavelength /Å	1.54056	0.71073	1.54056	1.54056
$2\Theta_{min}$ /°	3		2	3
$2\Theta_{max}$ /°	80		100	100
psd step in 2Θ /°	0.2		0.2	0.1
time/step / sec	150		150	300
number of scans	1		1	1
R_p /%	2.996	R_1 = 4.32	3.768	2.172
R_{wp} /%	3.925		5.104	2.792
R_{exp} /%	3.248		3.188	2.109
GOF	1.208		1.601	1.324
R_p' /% [a]	8.133		13.723	9.449
R_{wp}' /% [a]	8.579		13.588	9.075
R_{exp}' /% [a]	7.099		8.487	6.855
a) R_p', R_{wp}' and R_{exp}' values are background corrected according to the reference [38].				

Table S3. Crystallographic data of $[M^{II}Cl_2(3\text{-CNpy})_1]_n$ (**1b, 3b-5b**).

	1b	**3b**	**4b**	**5b**
Compound	$[MnCl_2(3\text{-CNpy})_1]_n$	$[CoCl_2(3\text{-CNpy})_1]_n$	$[NiCl_2(3\text{-CNpy})_1]_n$	$[CuCl_2(3\text{-CNpy})_1]_n$
CCDC number/ CSD code	1904108	1904114	1904109	1904115
Structure determined from	Powder	Powder	Powder	Powder
Formula	$C_6H_4Cl_2MnN_2$	$C_6H_4Cl_2CoN_2$	$C_6H_4Cl_2NiN_2$	$C_6H_4Cl_2CuN_2$
MW /g·mol^{-1}	229.95	233.95	233.71	238.56
Crystal system	Monoclinic	Orthorhombic	Orthorhombic	Monoclinic
Space group (No.)	*P nma* (62)	*P nma* (62)	*P nma* (62)	*P* $2_1/c$ (14)
***a* /Å**	16.5338(9)	16.0863(5)	15.9026(4)	3.7753(8)
***b* /Å**	3.693(12)	3.5874(10)	3.5328(6)	13.9311(4)
***c* /Å**	14.4596(9)	14.1910(5)	14.0807(4)	15.6849(3)
***α* /°**	90	90	90	90
***ß* /°**	90.0	90	90	96.114(3)
***γ* /°**	90	90	90	90
***V* /Å^3**	882.96(3)	818.9(1)	791.0(5)	820.2(4)
Z, Z'	4, ½	4, ½	4, ½	4, 1
Site symmetry of M^{II}	*.m.*	*.m.*	*.m.*	1
T /K	298	298	298	298
Radiation type	Mo $K\alpha_1$	Mo $K\alpha_1$	Cu $K\alpha_1$	Cu $K\alpha_1$
Wavelength /Å	0.70930	0.70930	1.54056	1.54056
$2\Theta_{min}$ /°	1.5	1.5	3	3
$2\Theta_{max}$ /°	60	60	80	80
psd step in 2Θ /°	0.21	0.21	0.2	0.2
time/step / sec	120	150	150	120
number of scans	1	1	1	1
***R_p* /%**	2.919	3.106	2.855	3.327
***R_{wp}* /%**	3.846	4.135	3.949	4.454
***R_{exp}* /%**	3.038	3.416	2.235	3.037
GOF	1.266	1.211	1.767	1.467
***R_p'* /% [a]**	10.620	11.498	8.994	6.172
***R_{wp}'* /% [a]**	11.042	11.403	10.396	7.176
***R_{exp}'* /% [a]**	8.722	9.419	5.883	4.893
a) R_p', R_{wp}' and R_{exp}' values are background corrected according to the reference [38].				

Text S1

Details on syntheses of $[M^{II}Cl_2(3\text{-}CNpy)_2]_{(n)}$

Synthesis of $[MnCl_2(3\text{-}CNpy)_2]_n$ (1a). $MnCl_2 \cdot 4\ H_2O$ (0.5 g, 2.53 mmol) was dissolved in 10mL ethanol, 3-CNpy (1.06 g, 10.18 mmol) was dissolved in 20 mL ethanol. By mixing both solutions, a colorless powder was obtained immediately. IR (cm^{-1}): 3101(w), 2236(m), 1595(m), 1473(s), 1417(s), 1043(m), 1037(m), 806(s), 689(s), 644(s).

Synthesis of $[FeCl_2(3\text{-}CNpy)_2]_n$ (2a). $FeCl_2 \cdot 4\ H_2O$ (2.5 g, 12.57 mmol) was dissolved in 20mL ethanol, 3-CNpy (2.5 g, 24.01 mmol) was dissolved in 20 mL ethanol. By mixing both solutions, a yellow powder was obtained within 12 hours IR (cm^{-1}): 3073(m), 2237(s), 1596(s), 1473(s), 1421(s), 1044(m), 1036(m), 815 (s), 690(s), 648(s).

Synthesis of $[CoCl_2(3\text{-}CNpy)_2]_n$ (3a). $CoCl_2 \cdot 6\ H_2O$ (1,0 g, 4,2 mmol) was dissolved in 10 mL methanol, 3-CNpy (0.44 g, 4.4 mmol) was dissolved in 20 mL methanol. By mixing both solutions, a light violet powder was obtained immediately. IR (cm^{-1}): 3068(m), 2238(m), 1599(m), 1473(s), 1045(m), 1036(m), 815(s), 689(s), 651(s).

Synthesis of $[NiCl_2(3\text{-}CNpy)_2]_n$ (4a). $NiCl_2 \cdot 6\ H_2O$ (1,0 g, 4,21 mmol) was dissolved in 15 mL methanol, 3-CNpy (0.44 g, 4.4 mmol) was dissolved in 10 mL methanol. By mixing both solutions, a light green powder was obtained immediately. IR (cm^{-1}): 3070(w), 2237(m), 1600(m), 1473(s), 1419(s), 1047(m), 1038(m), 814(s), 688(s), 653(s).

Synthesis of $[CuCl_2(3\text{-}CNpy)_2]_n$ (5a). $CuCl_2 \cdot 2\ H_2O$ (0,5 g, 2,93 mmol) was dissolved in 25 mL ethanol, 3-CNpy (1.30 g, 15.8 mmol) was dissolved in 15 mL ethanol. By mixing both solutions, an azure blue powder was obtained immediately. IR (cm^{-1}): 3066(w), 2237(m), 1601(m), 1472(s), 1419(s), 1049(m), 1034(m), 820(s), 687(s), 659(m).

Synthesis of $[ZnCl_2(3\text{-}CNpy)_2]$ (α-6a/ β-6a). $ZnCl_2 \cdot 4\ H_2O$ (0,46 g, 2,22 mmol) was dissolved in 3 mL ethanol, 3-CNpy (1.56 g, 15.04 mmol) was dissolved in 6 mL ethanol. The mixture was put in a fridge (~8 °C), and a colorless needle shaped powder (**α-6**) was obtained after slow evaporation of ethanol during two days. **α-6a** transforms within several hours at room temperature into **β-6a.** IR of the mixture

(cm^{-1}): 3112(w), 3055(w), 2242(w), 1614(s), 1495(m), 1417(s), 1064(s), 1027(s), 824(s), 672(m).

Text S2

Details on preparation of $[M^{II}Cl_2(3\text{-}CNpy)_1]_n$

Preparation of $[MnCl_2(3\text{-}CNpy)_1]_n$ (1b). 1b was prepared by thermal decomposition of $[MnCl_2(3\text{-}CNpy)_2]_n$ (**1a**). A light brown powder was obtained. Unfortunately, **1b** could not be prepared as pure phase and the measured sample contains a small quantity of $[MnCl_2(3\text{-}CNpy)_{1/3}]_n$. IR of the mixture ($cm^{-1}$): 2237(m), 1603(s), 1473(s), 1420(s), 1045(m), 1042(s), 816 (m), 690(s), 646(s).

Preparation of $[CoCl_2(3\text{-}CNpy)_1]_n$ (3b). 3b was prepared by thermal decomposition of $[CoCl_2(3\text{-}CNpy)_2]_n$ (**3a**)**.** A light violet powder was obtained. IR (cm^{-1}): 3067(w), 2237(m), 1598(s), 1473(s), 1420(s), 1045(m), 1036(m), 815 (m), 687(s), 650(s).

Preparation of $[NiCl_2(3\text{-}CNpy)_1]_n$ (4b). 4b was prepared by thermal decomposition of $[NiCl_2(3\text{-}CNpy)_2]_n$ (**4a**). An ochre powder was obtained. IR (cm^{-1}): 3065(w), 2237(m), 1603(s), 1468(s), 1420(s), 1037(m), 809(s), 689(s), 656(m).

Preparation of $[CuCl_2(3\text{-}CNpy)_1]_n$ (5b). 5b was prepared by thermal decomposition of $[CuCl_2(3\text{-}CNpy)_2]_n$ (**5a**)**.** A light blue powder was obtained. Several heating procedures with different temperatures and rates were performed in order to prepare $[CuCl_2(3\text{-}CNpy)_1]_n$ as pure phase, but remained unsuccessful. Temperature dependent XRPD experiments revealed, that $[CuCl_2(3\text{-}CNpy)_1]_n$ decomposes likely into $[CuCl_2(3\text{-}CNpy)_{1/3}]_n$ or CuCl and could not be prepared on the diffractometer instead (see Fig. S15). IR of the mixture (cm^{-1}): 3063(w), 2237(w), 1603(m), 1477(s), 1416(m), 1071(m), 1034(m), 815(s), 688(s), 659(s).

Text S3

Further details on structure solution and Rietveld refinements.

$[MnCl_2(3\text{-}CNpy)_2]_n$ (1a). The first 20 peaks were selected for indexing in DASH which resulted in an orthorhombic unit cell with Z = 2. Structure solution was carried out using simulated annealing with DASH. The molecular fragment ($MnCl_2(3\text{-}CNpy)_1$)

was restricted to rotate around the Mn atom on special position (0,0,0). The Cl atom was fixed on x = 0.5 during the refinement.

$[MnCl_2(3\text{-}CNpy)_1]_n$ (1b). At first, a Pawley fit was performed in TOPAS refining background and instrumental parameters (zero point, axial divergence). Next, size and strain parameters were refined. The crystal structure crystal structure of $[NiCl_2(3\text{-}CNpy)_1]_n$ was used as starting point for the subsequent structure refinement.

$[FeCl_2(3\text{-}CNpy)_2]_n$ (2a). The first 20 peaks were selected for indexing in CONOGRAPH which resulted in a monoclinic unit cell with Z = 4. Structure solution was carried out using simulated annealing with DASH. The molecular fragment ($FeCl_2(3\text{-}CNpy)_1$) was restricted to rotate around the Fe atom on special position (0,0,0).

$[CoCl_2(3\text{-}CNpy)_2]_n$ (3a). At first, a Pawley fit was performed in TOPAS (Coelho, 2018), refining background and instrumental parameters (zero point, axial divergence). Next, size and strain parameters were refined. The crystal structure of $[NiCl_2(3\text{-}CNpy)_2]_n$ (**4a**) was used as starting point for the subsequent structure refinement.

$[CoCl_2(3\text{-}CNpy)_1]_n$ (3b). At first, a Pawley fit was performed in TOPAS, refining background and instrumental parameters (zero point, axial divergence). Next, size and strain parameters were refined. The crystal structure of $[NiCl_2(3\text{-}CNpy)_1]_n$ was used as starting point for the subsequent structure refinement.

$[NiCl_2(3\text{-}CNpy)_2]_n$ (4a). At first, a Pawley fit was performed in TOPAS, background and instrumental parameters (zero point, axial divergence). Next, size and strain parameters were refined. The crystal structure of $[NiBr_2(3\text{-}CNpy)_2]_n$ [1] was used as starting point for the subsequent structure refinement.

$[NiCl_2(3\text{-}CNpy)_1]_n$ (4b). The first 20 peaks were selected for indexing in CONOGRAPH which resulted in an orthorhombic unit cell with Z = 4. Structure solution was carried out using simulated annealing in DASH. A molecular starting model was derived from the crystal structure of $[NiCl_2(3\text{-}CNpy)_2]_n$. The Ni atom and the pyridine ring were placed on special position ((x,1/4,z)) and the molecular fragment ($NiCl_2(3\text{-}CNpy)_1$) was restricted to rotate around the Ni atom during the simulated annealing. The Ni atom and the pyridine ring were fixed on y = 1/4 and the Cl atoms were fixed on y = 3/4 during the refinement.

$[CuCl_2(3\text{-}CNpy)_2]_n$ (5a). At first, a Pawley fit was performed in TOPAS, refining background and instrumental parameters (zero point, axial divergence). Next, size and strain parameters were refined. The single crystal structure [20] was used as starting point for the subsequent structure refinement.

$[CuCl_2(3\text{-}CNpy)_1]_n$ (5b). The first reliable 20 peaks were selected for indexing in DASH which resulted in a monoclinic unit cell with Z = 2. Structure solution was carried out using simulated annealing with DASH. The molecular fragment ($CuCl_2(3\text{-}CNpy)_1$) was restricted to rotate around the Cu atom.

α-$[ZnCl_2(3\text{-}CNpy)_2]$ (α-6a). The first 20 peaks were selected for indexing in CONOGRAPH which resulted in an orthorhombic unit cell with Z = 4. Structure solution was carried out using simulated annealing with DASH. A starting molecular model was derived from the crystal structure of $[ZnBr_2(3\text{-}CNpy)_2]$ [28]. The Zn and Cl atoms were placed on special position ((x,1/4,z)); the molecular fragment was restricted to rotate around the Zn atom during simulated annealing. Rietveld refinement was carried out with TOPAS. The Zn and Cl atoms were fixed on y = 1/4. Preferred orientation ([010]) was observed and thus refined.

β-$[ZnCl_2(3\text{-}CNpy)_2]$ (β-6a). The first 20 peaks were selected for indexing in CONOGRAPH, which resulted in a monoclinic unit cell with Z = 4. Structure solution was carried out using simulated annealing in DASH using a starting molecular model derived from the crystal structure of α-$[ZnCl_2(3\text{-}CNpy)_2]$ (**α-6a**). The molecular fragment was restricted to rotate around the Zn atom. Rietveld refinement was carried out with TOPAS. The Zn and Cl atoms were fixed on y = 1/4.